Theoretical and Applied Fracture Mechanics 125 (2023) 103944

Contents lists available at ScienceDirect

Theoretical and Applied Fracture Mechanics

journal homepage: www.elsevier.com/locate/tafmec

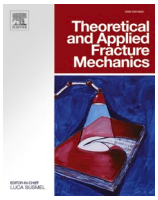

Crack tunneling effects on the elastic unloading compliance of C(T), SE(B) and clamped SE(T) specimens and correction methodology

L.G.F. Andrade [a,*], M. Mattar Neto [b], G.H.B. Donato [a]

[a] Centro Universitário FEI, São Bernardo do Campo, Brazil
[b] Instituto de Pesquisas Energéticas e Nucleares, IPEN–CNEN/SP, São Paulo, Brazil

ARTICLE INFO

Keywords:
Crack tunneling
Compliance
C(T)
SE(B)
Clamped *SE(T)*

ABSTRACT

This paper covers the effects of crack tunneling on *SE(B)*, *C(T)*, and clamped *SE(T)* specimens and presents a correction methodology for this effect and is divided in two parts. Part one presents an investigation of how crack front curvature affects instantaneous crack size predictions based on the elastic unloading compliance technique. Relative crack depths (a/W) of *0.2*, *0.5*, and *0.7*, were considered alongside five levels of crack curvature. Refined finite element models provided load-*CMOD* records in order to support compliance assessment. The crack front was modeled as a semi-ellipse, and the compliance results agreed with experimental data from the literature. It was shown that for the same equivalent physical straight crack standardized by *ASTM*, compliance generally decreases as tunneling increases. Since the maximum crack curvature allowed by the aforementioned standards is very restrictive, compliance did not meaningfully change within that limit, however, if violated, this paper shows that higher deviations may occur, leading to inaccurate crack depth estimations and invalid test results. These limits and deviations were clearly determined and, as a step to improve the techniques, this paper also presents – in part two – an exploration of a possible approach to mitigate this problem, which is based on the modification of how the equivalent straight crack of a curved crack front is determined. This new approach presents reduced errors in compliance-based crack size estimation as crack curvature increases when compared to current standardized protocols, and it can support further investigations in order to validate and standardize improved measuring techniques. Finally, it is important to state that even though the *ASTM* E1820 is used for the determination of crack driving forces, this study is based only on the study of the crack front curvature, the limit imposed by this standard and the deviations on crack size estimation when those limits are violated, while not focusing on determining errors directly on the J-integral. This paper is a further development on the studies published before by the research group.

1. Introduction

Advances in materials science in recent decades have led to advanced alloys that combine high strength and toughness. To fully understand how these materials behave and guarantee safe and reliable applications, a fracture mechanics approach to design is usually necessary. In fracture mechanics, both fatigue crack growth (da/dN-ΔK or ΔJ) and resistance curves (R-curves) are highly dependent on the instantaneous crack size throughout the tests, which can be predicted using techniques such as the elastic unloading compliance, with available current standards [1–3]. This technique correlates the specimen compliance (or stiffness inverse, V/P) with the crack size [4], therefore the greater the crack size, the higher the compliance.

Clarke et al. [5] were among the pioneers to develop a correlation between compliance and crack size with the ultimate objective of measuring a critical J value for crack stable extension (J_{IC}). A contribution of that study is the conclusion that a *10%* unloading to measure compliance would not affect J values. Studies with *C(T)* [6,7] and *SE(B)* [8,9] geometries were conducted in the following years showing great success in the application of the technique. On the other hand, studies with *SE(T)* are fairly recent. As stated by Cravero, Bravo and Ernst [10], this geometry has become popular due to the similarities of the stress profiles when compared to cracked pipelines. Moreira [11] developed one of the most comprehensive studies focused on the $SE(T)_c$ compliance.

From a standardized perspective, *SE(T)* geometry is covered by the British Institution *BS 8571* [12] for fracture toughness determination. In

* Corresponding author at: Humberto de Alencar, Castelo Branco Avenue, 3972-B - Assunção, São Bernardo do Campo, SP 09850-901, Brazil.
E-mail address: leonardogfa@gmail.com (L.G.F. Andrade).

https://doi.org/10.1016/j.tafmec.2023.103944
Received 20 November 2022; Received in revised form 15 April 2023; Accepted 22 May 2023
Available online 23 May 2023

Nomenclature

Latin

a	Crack depth (mm)
a/W	Relative crack depth (mm/mm)
a/W_{DELTA}	Relative crack depth variation (%)
a/W_0	Straight crack ($T = 0\ mm$) relative crack depth estimation (mm/mm)
B	Thickness (mm)
C	Compliance (mm/N)
C_{DELTA}	Compliance variation (%)
C_0	Straight crack ($T = 0\ mm$) compliance (mm/N)
$C(T)$	Compact under tension specimen
da/dN	Fatigue crack growth rate
E	Elastic modulus (GPa)
H	$SE(T)$ daylight length (mm)
J	J integral. Non-linear energy release rate (J/mm^2)
J_{IC}	Critical J integral for the start of stable extension of the crack (J/mm^2)
$SE(B)$	Single-edge-notched under bending specimen
$SE(T)$	Single-edge-notched under tension specimen
T	Tunneling level (mm)
T/B	Relative tunneling level (mm/mm)
V	Crack mouth opening displacement (mm)
W	Width (mm)

Greek

β	Weights for the points of measurement used for determining the equivalent crack front
ν	Poisson's ratio
μ	Normalized compliance

this standard, the elastic compliance technique is allowed for measuring the crack size in single specimen tests with the condition that it should be validated by a multiple specimen R-curve. *ASTM* standardization is still pending.

Furthermore, recommended practices for testing the *SE(T)* can be found on the literature. Such documents are usually related to the oil and gas and other high responsibility industries and are guidelines for evaluating fracture mechanics parameters with the *SE(T)* geometry. Most of those practices allows the elastic compliance technique for crack size measurement in single specimen tests. Exemplifying:

- Det Norske Veritas' *DNV-RP-F108* [13];
- CanMET Materials Technology Laboratory – Fracture toughness testing using *SE(T)* samples with fixed-grip loading [14];
- ExxonMobil Upstream Research Company – Fracture resistance curves using single-edge notched tension specimens [15].

Even though the compliance technique is widely employed in fracture mechanics tests, some effects may affect its accuracy. Among those are: rotation [16], side grooves, relative thickness and stress triaxiality [11], plasticity [17] and crack tunneling [18–19]. This paper addresses the latter, a phenomenon that occurs when the crack grows deeper in the center portion of a specimen and shallower at the edges due to different stress states ahead of the crack, with plane strain (more severe) prevailing in the center and plane stress (less severe) at the edges. This may lead the crack, once straight, to form a shape close to a semi-ellipse, and therefore uneven crack depth alongside the thickness of the specimen [4]. Steenkamp [20] was one of the first to evaluate how tunneling impacts compliance in *SE(B)* specimens. That study shows that compliance would be reduced as the curvature of the crack increased for the same equivalent crack depth. More recent studies conducted by Yan and Zhou [18] on *SE(B)* specimens and by Huang and Zhou [19] on $SE(T)_c$ specimens demonstrate the same trend, with compliance decreasing with increasing curvature. Both studies used modern simulation tools and highly refined three-dimensional meshes to model and test the specimens. In addition, the crack front was modeled with an equation proposed by Nikishkov, Heerens and Hellmann [21], based on the postmortem observation of various tunneled *C(T)* specimens. The result was a crack front description close to a semi-ellipse.

It is important to emphasize that the elastic unloading compliance is broadly used in many fracture mechanics studies, as exemplified on [22,23] and more recently on [24,25]. A wide range review of compliance solutions can be found on [26]. Based on the relevance of such technique, understanding how the crack front curvature affects the crack depth predictions could positively impact fracture mechanics applications and results.

The authors would like to point out that this article contains, in its first part, an in-depth study of the of crack tunelling effects on the elastic unloading compliance of C(T), SE(B) and clamped SE(T) specimens, followed by the proposal and exploratory numerical validation of a methodology for developing correction techniques. Such further investigations are advances in relation to initial studies restricted to SE(B) specimens published by the research group in [27]. The current work, thus, evaluates in more details the effects of crack tunneling on SE(B) and two additional geometries – C(T) and clamped SE(T) - and openly presents the proposal development methodology for the scientific community, aiming to thoroughly develop it.

1.1. ASTM equivalent straight crack and β coefficients

According to *ASTM E1820* [1], the physical measuring of the initial, final, and intermediate (when possible) crack sizes should be performed after the test has ended and the two pieces of the specimen are separated. The crack should be measured at nine equidistant points, with one in the center and two *0.005 W* from the edges of the specimen. Next, the average of the two points closest to the edges is calculated and finally, the arithmetical average of the remaining eight values determines the average crack size. The equivalent straight crack can also be determined in terms of relative crack depth for convenience, and is shown below:

$$a/W_{eq} = \frac{\frac{(a/W_1 + a/W_9)}{2} + \sum_{i=2}^{8} a/W_i}{8}, \tag{1}$$

where a/W_{eq} is the equivalent relative crack depth and a/W_i is the relative crack depth at the nine i^{th} points of measurement indicated by *ASTM E1820*. The maximum allowed curvature is defined by limiting the maximum difference between the nine points and the average to *5%* of the thickness (*0.05B*). If the difference is greater, the specimen and its results are invalidated.

If the crack is symmetrical, $a/W_1 = a/W_9$, $a/W_2 = a/W_8$, $a/W_3 = a/W_7$, $a/W_4 = a/W_6$, leading to:

$$a/W_{eq.sym.} = \frac{a/W_1 + \sum_{i=2}^{5}(2.a/W_i)}{8}, \tag{2}$$

and therefore:

$$a/W_{eq.sym.} = 0.125a/W_1 + 0.250a/W_2 + 0.250a/W_3 + 0.250a/W_4 + 0.125a/W_5. \tag{3}$$

β coefficients are now defined as the weights each measurement impacts on the equivalent crack size. For the *ASTM E1820* and symmetrical crack, $\beta_1 = \beta_5 = 0.125$ (center and edges) and $\beta_2 = \beta_3 = \beta_4 = 0.250$ (intermediate points).

Part 1: Crack tunneling effects on compliance.

2. Methodology

2.1. Geometry

C(T), *SE(B),* and $SE(T)_c$ were considered with a fixed width W of *50.8 mm*, three values of thickness B of *12.7*, *25.4,* and *50.8 mm* and three values of crack depth a/W of *0.2*, *0.5,* and *0.7* (respectively representing shallow, medium, and deep cracks). For the $SE(T)_c$, the daylight length H is fixed as *10* times the width. All the remaining dimensions follow the *ASTM E1820* recommendations [1]. In this paper, tunneling level *T (mm)* is interpreted as the longitudinal distance between the deepest and shallowest point of the crack front. This parameter was chosen due to proximities to laboratory measurement practices and quantitatively shows the tunneling level. In addition, all results presented below also shows the relative to the thickness T/B value, that has shown to be more robust for a proposal development perspective. All further studies will be based on T/B.

$$T = max(a/W_i) - min(a/W_i). \tag{4}$$

Crack front was modeled as a semi-ellipse, with geometries in accordance with the literature [18–19]. Five levels of tunneling were implemented in the specimen models by modifying the original straight crack mesh with a node coordinates manipulation algorithm, ensuring that the equivalent straight crack calculated by the *ASTM* method was the original crack depth before any modification to the mesh. Evaluated tunneling levels were *0*, *1*, *2*, *4,* and *6 mm*.

Considering all the geometry variations, *135* models were developed to determine the impact of tunneling on compliance.

2.2. Materials

Since the elastic unloading compliance technique is based only on elastic premises, a material following Hooke's Law is sufficient to evaluate and isolate tunneling effects. Based on such assumption, a model of a steel alloy with $E = 206\ GPa$ and $\nu = 0.3$ was considered. No plasticity was incorporated to the FEM material model.

It's important to state that the authors' research group employ plasticity and other more complex materials models such as *GTN* (damage model) in other ongoing compliance studies, but validations including plasticity revealed that the elastic model is sufficient for the intended assessments of this study.

2.3. FEM models

The adequate development of the finite elements model is key to reaching the main objective of this research. Element type and mesh size affect the results and simulation process time, and for this reason equilibrium is necessary. Huang and Zhou [19] utilized a highly refined *3-D* mesh with *20*-node hexahedral elements (*HEX20*) while Moreira [11] also used a highly refined *3-D* mesh but with *8*-node hexahedral elements (*HEX8*). The author determined that for linear elastic simulations, *HEX8* elements were just as accurate and would yield the same conclusions as *HEX20* elements with less simulation process time. A highly refined mesh (*6000–8000* elements and *7000–9000* nodes) and *HEX8* elements (*Abaqus*® [28] type *C3D8*) were chosen to construct the models. *10* elements with linearly varying size were used to describe the thickness of the models to properly describe the curvature (bigger elements on the center and smaller elements on the edges). An example of a model used in this paper is shown in Fig. 1.

The crack tip was modeled by a blunt mesh, with a radius of *0.05 mm*. No differences in results were observed when compared to smaller radius values such as *0.005 mm* and *0.0005 mm*, both with higher computational demands. This crack front description is in accordance with the literature [17–19]. One quarter of each specimen was modeled to save simulation time with the employment of usual double symmetry boundary conditions and therefore increase computational efficiency.

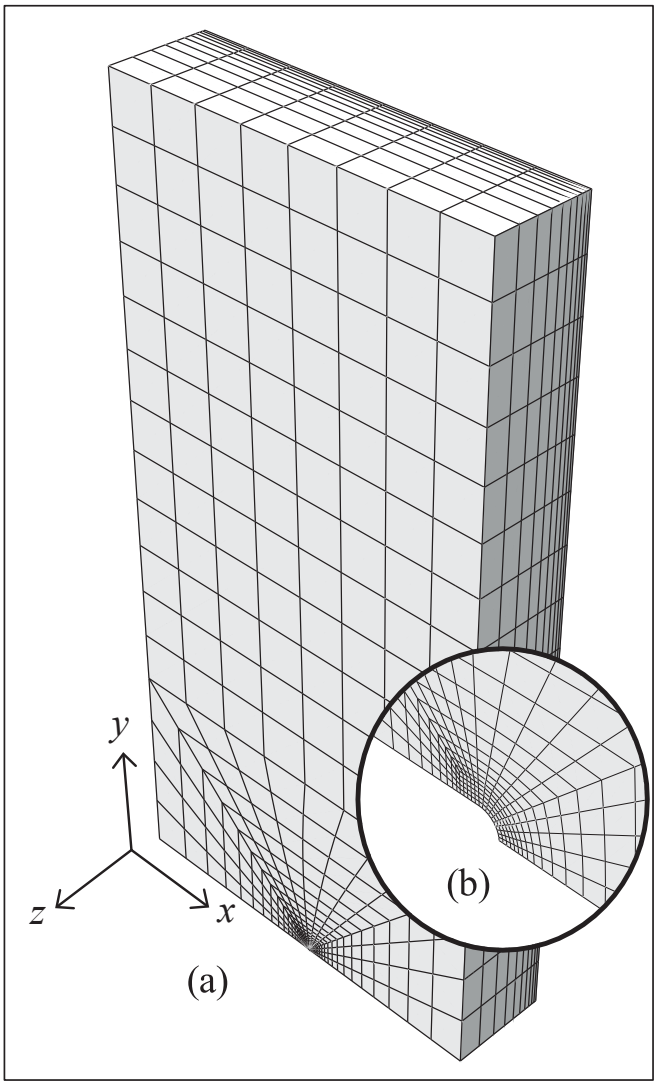

Fig. 1. (a)Example of a SE(B) model. (b) Blunt crack tip detail.

Even though linear elastic material is used, the simulations were conducted including nonlinear effects due to large geometry change. Loading was applied to the models as displacements at the locations described below. *0.002 mm* were added at each increment of the simulation according to each geometry configuration. In total, *100* increments were used, totalizing *0.2 mm* of total displacement.

a. *C(T)*: A rigid body representing the pin was created with proper frictionless contact with the inner surface of the pin hole of the model and load was applied via the rigid body.
b. *SE(B)*: Central nodes of the crack plane representing the center roller of the three-point bending device.
c. Clamped *SE(T)*: nodes of the top portion that represents the clamped regions in fixtures.

C(T) simulations used contact to load the specimen, contrary to the *SE(B)* that used nodal restriction. This was done because the first presented meaningful deviations even on linear elastic regimen.

It is worth noting that for assessments including non-linear material, plasticity effects and large geometry change, detailed contact modelling is desired and enhances the representativeness of the *SE(B)* simulation.

3. Results

In this section, the results for *SE(B)*, clamped *SE(T)*, and *C(T)* are shown. They are displayed as graphics showing the correlation of compliance delta (C_{DELTA}, Eq. (5)) with tunneling level T and relative tunneling level T/B. The maximum curvature allowed by the *ASTM E1820* [1] is also displayed as a vertical dashed line and is a function of the thickness. For $B = 50.8$ *mm*, the ASTM limit is $T = 4.04$ *mm* and $T/B = 0.0796$. For *25.4 mm*, $T = 2.17$ *mm* and $T/B = 0.0861$ and finally, for *12.7 mm*, $T = 1.23$ *mm* and $T/B = 0.0970$. Additionally, tables with detailed results of compliance, C_{DELTA}, a/W and a/W_{DELTA} (Eq. (6)) are shown.

Relative crack depth a/W was determined by the fifth order polynomial regression available on the *ASTM E1820* [1] for *SE(B)* and *C(T)* geometries. Since the $SE(T)_c$ is not an *ASTM* normalized geometry, the polynomial regression of Moreira's work (Eq. (7)) was used [11].

$$C_{DELTA} = \frac{(C - C_0)}{C_0}.100. \tag{5}$$

$$a/W_{DELTA} = \frac{(a/W - a/W_0)}{a/W_0}.100. \tag{6}$$

$$a/W_{MOREIRA} = -66.4646\mu^5 + 129.9279\mu^4 - 99.6375\mu^3 + 39.67951\mu^2 - 10.1233\mu + 1.7158. \tag{7}$$

3.1. Se(B)

Analysis of the results for the *SE(B)* shows that there is a clear trend for an increase in compliance within *ASTM E1820* [1] limits and a posterior decrease with higher crack curvatures. Similar behavior can be observed in Yan and Zhou's work [18] for the same geometry. Even with the increase, compliance values, and therefore crack depth estimation, did not change significantly within *ASTM E1820* limits (highest amount of error is -1.63% in compliance yielding -1.37% in relative crack size prediction through the fifth order polynomial regression), although when this condition is violated more substantial errors can be seen as presented by Figs. 2 to 4 and respective Tables 1 to 3. Highest detected error is for high tunneling and thin specimen ($B = 12.7$ *mm*, $T = 6$ *mm*, Table 3), with values of *11.1%* and *9.46%* decrease in compliance and predicted a/W respectively. It is also important to state that the average crack depth ($a/W = 0.5$) yielded the lowest absolute amount of error when compared to the others. This is systematically observed in all studied cases regardless of specimen type or W/B, and this behavior will be scope of further studies.

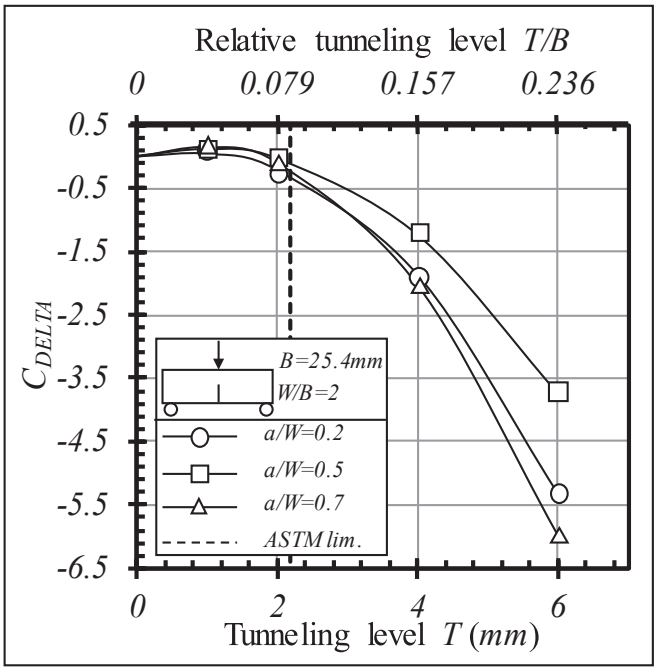

Fig. 3. C_{DELTA} versus tunneling level for the SE(B) B = 25.4 mm.

3.2. $SE(T)_c$

Analogous to the *SE(B)* geometry, the same behavior was seen for the $SE(T)_c$, (Figs. 5 to 7 and Tables 4 to 6) with a slight increase in compliance within the *ASTM E1820* [1] limit and a subsequent more intense reduction as tunneling increases. In addition, results are

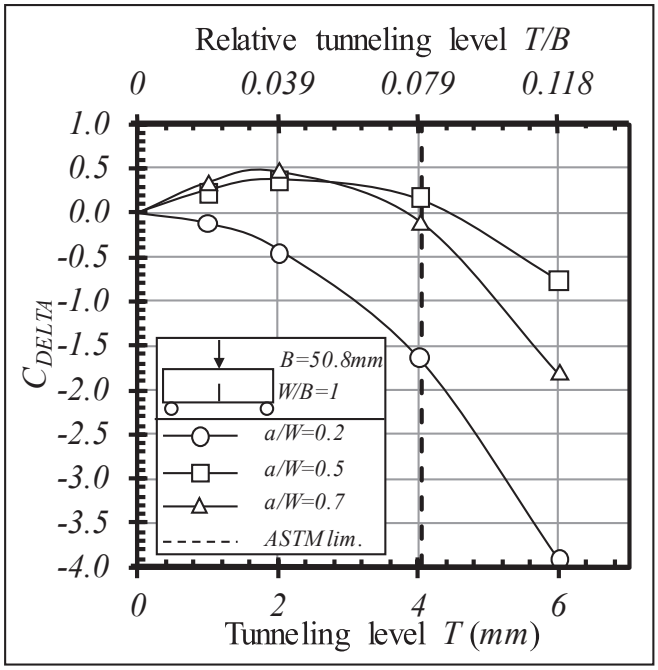

Fig. 2. C_{DELTA} versus tunneling level for the SE(B) B = 50.8 mm.

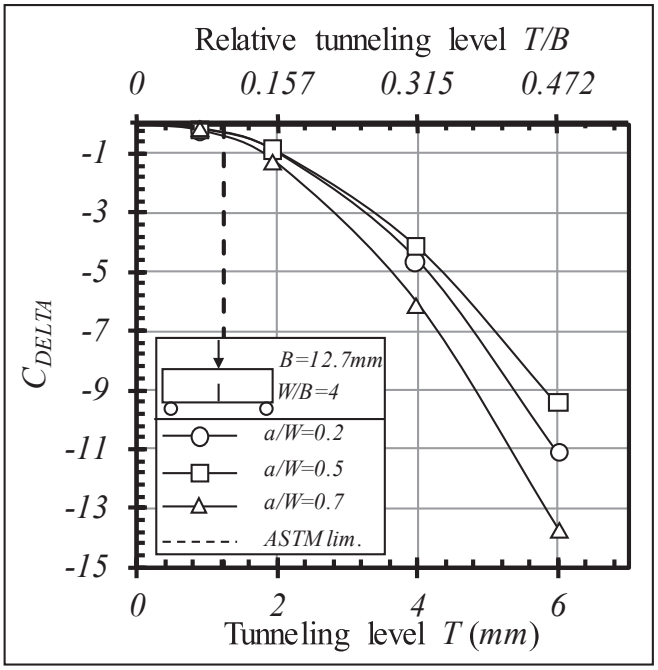

Fig. 4. C_{DELTA} versus tunneling level for the SE(B) B = 12.7 mm.

Table 1
Results for SE(B) specimen, W/B = 1. All a/W and T levels.

Model a/W	T level	Compliance	C_{DELTA}	$a/W_{predicted}$	a/W_{DELTA}
(mm/mm)	(mm)	(mm/N)	%	(mm/mm)	%
0.2	0	6.42E-07	n/a	0.192	n/a
	1	6.42E-07	−0.12	0.192	−0.10
	2	6.40E-07	−0.41	0.191	−0.34
	4	6.32E-07	−1.63	0.189	−1.37
	6	6.17E-07	−3.91	0.185	−3.31
0.5	0	3.20E-06	n/a	0.488	n/a
	1	3.21E-06	0.25	0.489	0.09
	2	3.21E-06	0.37	0.489	0.14
	4	3.20E-06	0.15	0.489	0.06
	6	3.17E-06	−0.76	0.487	−0.29
0.7	0	1.14E-05	n/a	0.69	n/a
	1	1.15E-05	0.35	0.69	0.07
	2	1.15E-05	0.47	0.691	0.09
	4	1.14E-05	−0.08	0.69	−0.02
	6	1.12E-05	−1.81	0.688	−0.35

Table 2
Results for SE(B) specimen, W/B = 2. All a/W and T levels.

Model a/W	T level	Compliance	C_{DELTA}	$a/W_{predicted}$	a/W_{DELTA}
(mm/mm)	(mm)	(mm/N)	%	(mm/mm)	%
0.2	0	1.32E-06	n/a	0.196	n/a
	1	1.32E-06	0.04	0.196	0.03
	2	1.32E-06	−0.22	0.196	−0.18
	4	1.29E-06	−1.87	0.193	−1.56
	6	1.25E-06	−5.32	0.187	−4.49
0.5	0	6.56E-06	n/a	0.493	n/a
	1	6.56E-06	0.1	0.493	0.04
	2	6.56E-06	−0.04	0.493	−0.02
	4	6.48E-06	−1.24	0.491	−0.46
	6	6.31E-06	−3.72	0.486	−1.40
0.7	0	2.35E-05	n/a	0.693	n/a
	1	2.35E-05	0.15	0.693	0.03
	2	2.34E-05	−0.1	0.693	−0.02
	4	2.30E-05	−2.02	0.691	−0.39
	6	2.21E-05	−5.95	0.685	−1.17

comparable with Huang and Zhou's work [19] for the same geometry. The highest amount of compliance error within the *ASTM* limit was *−1.78%* and when limits are violated decreases in *a/W* prediction in the order of 3% to 8% are detected.

3.3. C(T)

Repeating what was observed for *SE(B)* and *SE(T)$_c$*, the same trend was detected for the *C(T)* (Figs. 8 to 10 and Tables 7 to 9). The highest

Table 3
Results for SE(B) specimen, W/B = 4. All a/W and T levels.

Model a/W	T level	Compliance	C_{DELTA}	$a/W_{predicted}$	a/W_{DELTA}
(mm/mm)	(mm)	(mm/N)	%	(mm/mm)	%
0.2	0	2.68E-06	n/a	0.198	n/a
	1	2.67E-06	−0.19	0.198	−0.16
	2	2.65E-06	−0.97	0.197	−0.80
	4	2.55E-06	−4.6	0.191	−3.85
	6	2.38E-06	−11.1	0.18	−9.46
0.5	0	1.33E-05	n/a	0.495	n/a
	1	1.32E-05	−0.21	0.494	−0.08
	2	1.31E-05	−0.95	0.493	−0.35
	4	1.27E-05	−4.19	0.487	−1.56
	6	1.20E-05	−9.51	0.477	−3.67
0.7	0	4.77E-05	n/a	0.696	n/a
	1	4.76E-05	−0.27	0.695	−0.05
	2	4.71E-05	−1.34	0.694	−0.25
	4	4.48E-05	−6.07	0.687	−1.18
	6	4.12E-05	−13.67	0.676	−2.81

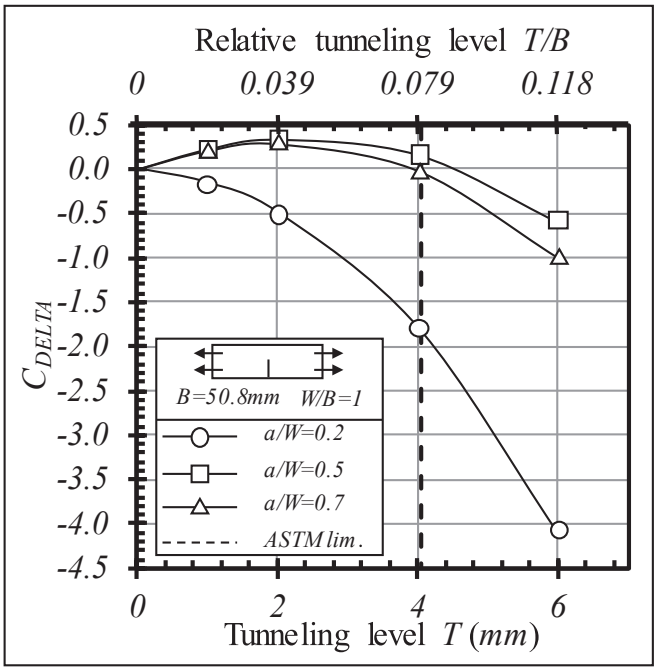

Fig. 5. C_{DELTA} versus tunneling level for the SE(T)$_c$ B = 50.8 mm.

amount of error within the *ASTM E1820* [1] limit was *−1.74%*. Particularly to the *C(T)*, thick *W/B = 1* and shallow *a/W = 0.2* specimen configuration presented atypical results of C_{DELTA} evolution with tunneling level. This is an extreme situation for this type of specimen, and the extreme loads could potentially mischaracterize the compact specimen load profile. This is an isolated case and deserves future investigation.

Even though all geometries studied have distinct dimensional, loading, and constraint characteristics, the general trend of the compliance evolution with increasing tunneling was the same. This indicates that an effect common to all three geometries could be causing the compliance to change as it does, and a possible answer to the

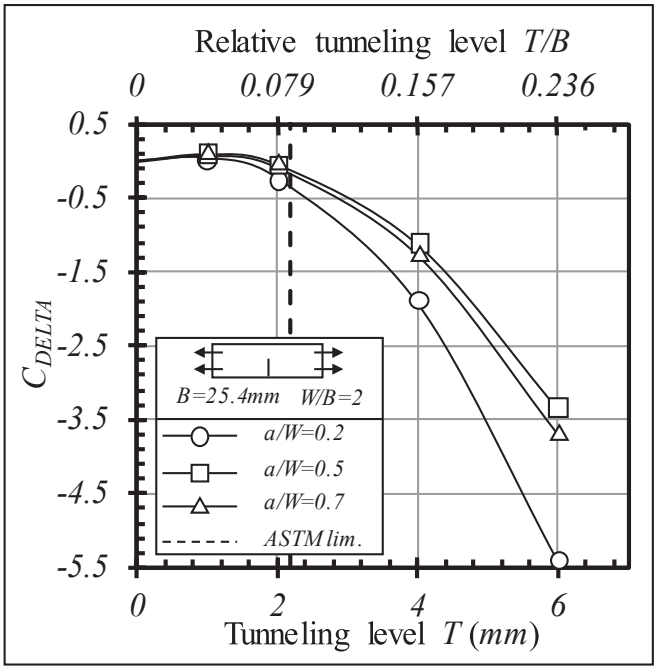

Fig. 6. C_{DELTA} versus tunneling level for the SE(T)$_c$ B = 25.4 mm.

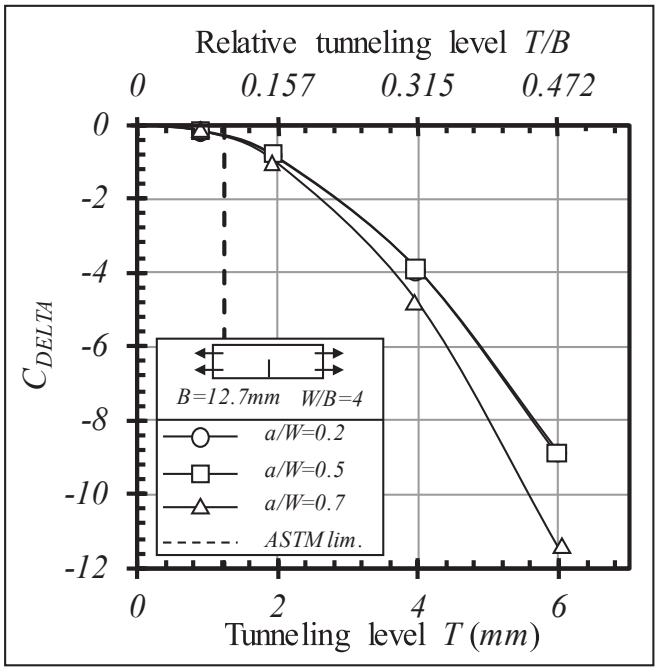

Fig. 7. C_{DELTA} versus tunneling level for the SE(T)$_c$ B = 12.7 mm.

Table 4
Results for SE(T)$_c$ specimen, W/B = 1. All a/W and T levels.

Model a/W	T level	Compliance	C_{DELTA}	$a/W_{predicted}$	a/W_{DELTA}
(mm/mm)	(mm)	(mm/N)	%	(mm/mm)	%
0.2	0	1.28E-07	n/a	0.202	n/a
	1	1.27E-07	−0.16	0.201	−0.12
	2	1.27E-07	−0.49	0.201	−0.36
	4	1.25E-07	−1.78	0.199	−1.30
	6	1.22E-07	−4.09	0.196	−3.00
0.5	0	6.85E-07	n/a	0.504	n/a
	1	6.87E-07	0.23	0.504	0.09
	2	6.88E-07	0.34	0.504	0.13
	4	6.86E-07	0.17	0.504	0.07
	6	6.81E-07	−0.6	0.502	−0.24
0.7	0	1.94E-06	n/a	0.714	n/a
	1	1.95E-06	0.21	0.715	0.06
	2	1.95E-06	0.29	0.715	0.08
	4	1.94E-06	−0.01	0.714	0.00
	6	1.93E-06	−0.99	0.712	−0.28

Table 5
Results for SE(T)$_c$ specimen, W/B = 2. All a/W and T levels.

Model a/W	T level	Compliance	C_{DELTA}	$a/W_{predicted}$	a/W_{DELTA}
(mm/mm)	(mm)	(mm/N)	%	(mm/mm)	%
0.2	0	2.61E-07	n/a	0.205	n/a
	1	2.61E-07	0.03	0.205	0.02
	2	2.61E-07	−0.24	0.205	−0.17
	4	2.56E-07	−1.93	0.202	−1.40
	6	2.47E-07	−5.42	0.197	−3.96
0.5	0	1.40E-06	n/a	0.507	n/a
	1	1.40E-06	0.09	0.507	0.03
	2	1.39E-06	−0.05	0.507	−0.02
	4	1.38E-06	−1.13	0.505	−0.44
	6	1.35E-06	−3.34	0.5	−1.33
0.7	0	3.94E-06	n/a	0.717	n/a
	1	3.94E-06	0.08	0.717	0.02
	2	3.93E-06	−0.08	0.717	−0.02
	4	3.89E-06	−1.27	0.714	−0.36
	6	3.79E-06	−3.69	0.709	−1.07

Table 6
Results for SE(T)$_c$ specimen, W/B = 4. All a/W and T levels.

Model a/W	T level	Compliance	C_{DELTA}	$a/W_{predicted}$	a/W_{DELTA}
(mm/mm)	(mm)	(mm/N)	%	(mm/mm)	%
0.2	0	5.29E-07	n/a	0.207	n/a
	1	5.28E-07	−0.2	0.207	−0.15
	2	5.24E-07	−1.03	0.206	−0.74
	4	5.04E-07	−4.79	0.200	−3.48
	6	4.69E-07	−11.43	0.189	−8.47
0.5	0	2.81E-06	n/a	0.509	n/a
	1	2.81E-06	−0.2	0.508	−0.08
	2	2.79E-06	−0.9	0.507	−0.35
	4	2.70E-06	−3.9	0.501	−1.56
	6	2.56E-06	−8.83	0.490	−3.60
0.7	0	7.94E-06	n/a	0.719	n/a
	1	7.93E-06	−0.19	0.718	−0.05
	2	7.87E-06	−0.87	0.717	−0.25
	4	7.63E-06	−3.91	0.711	−1.13
	6	7.23E-06	−8.94	0.700	−2.65

problem may reside in the geometrical configuration of the crack. When modeled with the *ASTM E1820* [1] configuration ($\beta_1 = \beta_5 = 0.125$ and $\beta_2 = \beta_3 = \beta_4 = 0.250$, Eq. (3)), the crack may favor a decrease in compliance for the analyzed conditions within the scope of this paper, as shown in the results above.

Part 2: A new approach for measuring the equivalent crack size.

The following sections show the methodology and results of an exploratory proposal for measuring and post-processing the curved crack profile. This is an effort to better correlate the equivalent straight crack with its corresponding compliance, which has the potential to validate specimens and results otherwise discarded by current *ASTM* standards because of excessive crack curvature. The exploratory approach is focused on determining systematically a group of β coefficients that reduce the compliance errors of curved cracks throughout the crack depth range.

4. Methodology

In Part 1, the β coefficients (Eq. (3), derived from *ASTM*) were used to find the position of the curved crack front. As shown in the results, this may cause deviations in compliance when compared to the equivalent

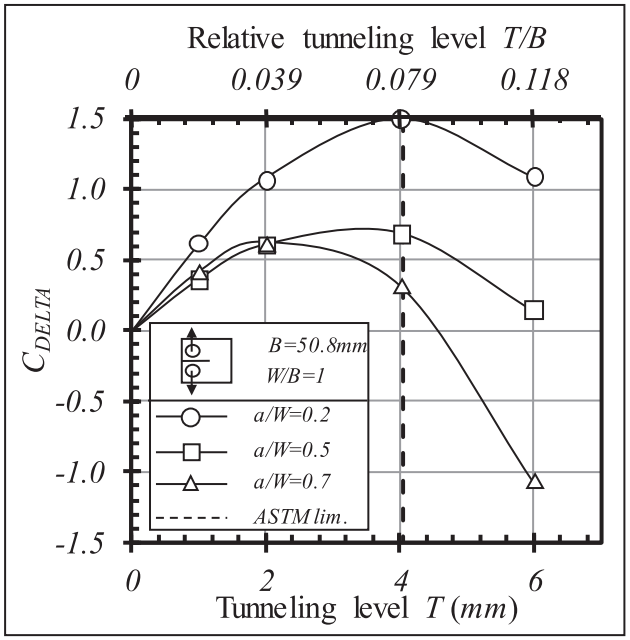

Fig. 8. C_{DELTA} versus tunneling level for the C(T) B = 50.8 mm.

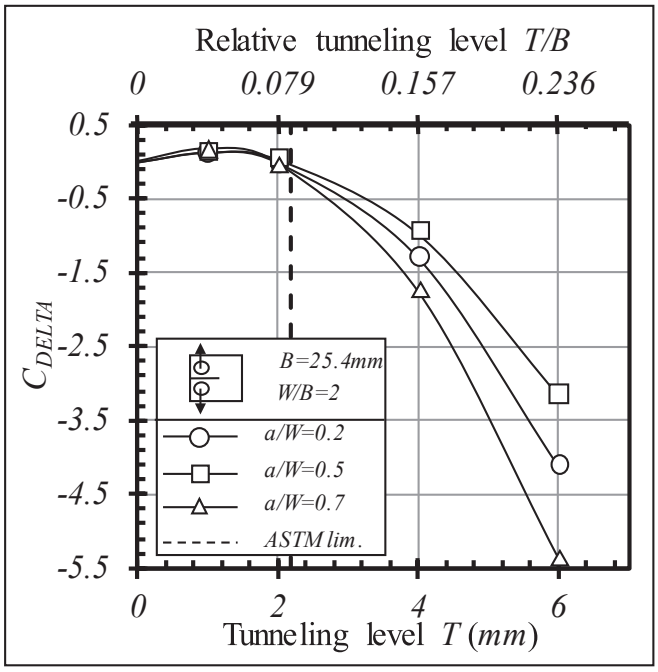

Fig. 9. C_{DELTA} versus tunneling level for the C(T) B = 25.4 mm.

straight crack according to the standard. The elaboration of this proposal begins by performing the inverse: starting by finding which position of the curved crack front would generate the same compliance as the straight crack, by offsetting the tunneled semi-elliptical crack with equivalent crack size determined by the *ASTM*, as shown in Fig. 11. This was performed for each tunneling level following the steps below.

a. Determine the straight crack compliance.
b. Design a semi-elliptical crack, for the desired *T* level, maintaining the same *ASTM* equivalent depth.

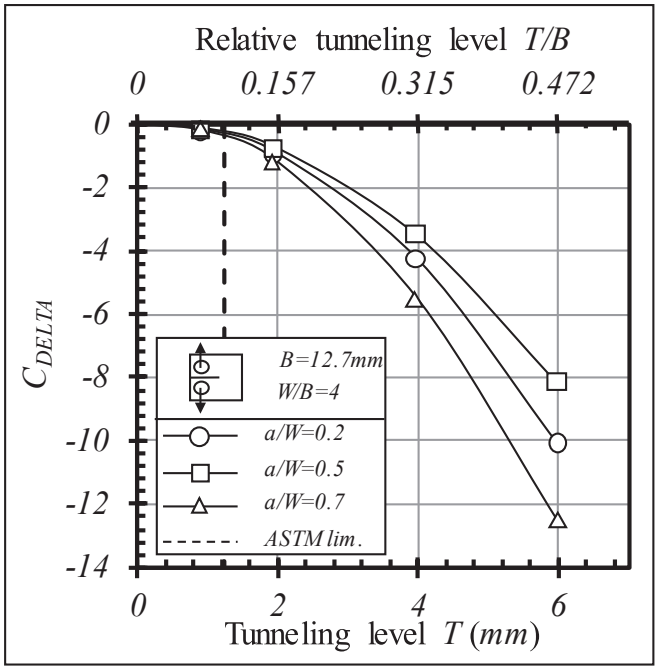

Fig. 10. C_{DELTA} versus tunneling level for the C(T) B = 12.7 mm.

Table 7
Results for C(T) specimen, W/B = 1. All a/W and T levels.

Model a/W	T level	Compliance	C_{DELTA}	$a/W_{predicted}$	a/W_{DELTA}
(mm/mm)	(mm)	(mm/N)	%	(mm/mm)	%
0.2	0	6.72E-07	n/a	0.162	n/a
	1	6.77E-07	0.61	0.163	0.72
	2	6.80E-07	1.08	0.164	1.26
	4	6.83E-07	1.50	0.165	1.74
	6	6.80E-07	1.09	0.164	1.27
0.5	0	3.26E-06	n/a	0.484	n/a
	1	3.27E-06	0.36	0.484	0.15
	2	3.28E-06	0.61	0.485	0.26
	4	3.28E-06	0.69	0.485	0.29
	6	3.26E-06	0.14	0.484	0.06
0.7	0	1.09E-05	n/a	0.69	n/a
	1	1.09E-05	0.41	0.69	0.08
	2	1.09E-05	0.62	0.691	0.12
	4	1.09E-05	0.32	0.690	0.06
	6	1.08E-05	−1.07	0.688	−0.21

Table 8
Results for C(T) specimen, W/B = 2. All a/W and T levels.

Model a/W	T level	Compliance	C_{DELTA}	$a/W_{predicted}$	a/W_{DELTA}
(mm/mm)	(mm)	(mm/N)	%	(mm/mm)	%
0.2	0	1.51E-06	n/a	0.184	n/a
	1	1.51E-06	0.13	0.184	0.14
	2	1.51E-06	−0.01	0.184	−0.01
	4	1.49E-06	−1.29	0.181	−1.33
	6	1.44E-06	−4.12	0.176	−4.30
0.5	0	6.79E-06	n/a	0.492	n/a
	1	6.80E-06	0.13	0.492	0.05
	2	6.80E-06	0.03	0.492	0.01
	4	6.73E-06	−0.97	0.490	−0.40
	6	6.58E-06	−3.14	0.486	−1.31
0.7	0	2.24E-05	n/a	0.694	n/a
	1	2.24E-05	0.17	0.694	0.03
	2	2.24E-05	−0.03	0.694	−0.01
	4	2.20E-05	−1.76	0.691	−0.35
	6	2.12E-05	−5.34	0.686	−1.08

c. Offset the crack position along the width, run the simulation and determine the model compliance. Very small offset values are used here (*-0.2* to *0.2 mm*, in *0.05 mm* steps).
d. Generate a compliance *vs.* offset graph and, through a linear regression (that is shown adequate for very small offsets), determine the exact value that would provide the same compliance as the straight crack.

Table 9
Results for C(T) specimen, W/B = 4. All a/W and T levels.

Model a/W	T level	Compliance	C_{DELTA}	$a/W_{predicted}$	a/W_{DELTA}
(mm/mm)	(mm)	(mm/N)	%	(mm/mm)	%
0.2	0	3.09E-06	n/a	0.188	n/a
	1	3.08E-06	−0.2	0.188	−0.20
	2	3.06E-06	−0.94	0.186	−0.94
	4	2.95E-06	−4.28	0.18	−4.36
	6	2.78E-06	−10.10	0.168	−10.63
0.5	0	1.38E-05	n/a	0.495	n/a
	1	1.37E-05	−0.16	0.494	−0.07
	2	1.36E-05	−0.78	0.493	−0.32
	4	1.33E-05	−3.56	0.487	−1.48
	6	1.26E-05	−8.23	0.477	−3.52
0.7	0	4.56E-05	n/a	0.696	n/a
	1	4.55E-05	−0.24	0.696	−0.05
	2	4.50E-05	−1.21	0.694	−0.23
	4	4.30E-05	−5.53	0.688	−1.11
	6	3.99E-05	−12.52	0.678	−2.64

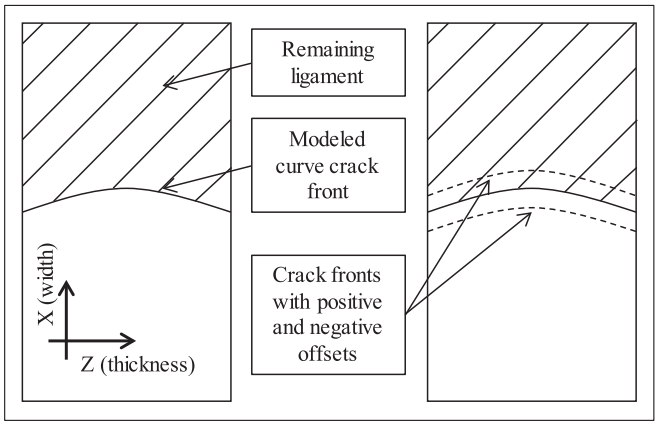

Fig. 11. Example of tunneled cracks with offset.

e. Generate a model with the exact offset found in item (d) to validate the desired compliance. At this point, the compliance of the curved offset crack should be within *0.001%* of the straight crack (a).
f. Repeat for all studied tunneling levels.

The positions of the curved cracks that yields the same compliance as the straight crack's counterparts are now defined. Please note that the cracks have the same profile but not the same position. At this point, if Eq. (3) is employed to calculate the equivalent straight crack, the initial a/W will not be maintained. With that, it is now possible to calculate the error that the *ASTM* β coefficients causes. The error is defined as the absolute difference between the desired a/W and the predicted a/W (Eq. (8)). The evolution of the error with increasing tunneling level for the *SE(B), B = 25.4, a/W = 0.5* is shown in Fig. 12.

$$Error = |a/W_{desired} - a/W_{predicted}| \tag{8}$$

That enables the determination of the best combination of β coefficients that provides the least amount of error for each tunneling level. After that, in an effort to find one single group of β coefficients that fits the model thorough all curvatures, the errors of all tunneling levels were summed and minimized using a GRG non-linear algorithm. The β coefficients were the only parameters to vary, and the boundary condition was that their sum should be equal to the unity. Unfortunately for all cases analyzed, even though the sum of the errors was lower than the *ASTM*, the errors in the less curved cracks were significantly higher, leading to a still unfavored scenario. Fig. 13 shows the errors graphically for the same model.

A new approach to the problem was then elaborated. Instead of using the β coefficients as fixed weights, they can be interpreted as functions of the tunneling level T. Instead of using the GRG nonlinear algorithm to minimize the errors for all tunneling levels together, the algorithm can be used to find a group of β coefficients for each tunneling level. The group of β coefficients for the *SE(B), B = 25.4 mm, a/W = 0.5* is shown below in Table 10. Finally, a graph of the evolution of the β coefficients with tunneling level can be generated (Fig. 14). With a linear regression (least squares fit) all the values of β coefficients can now be written as a function of the tunneling level T as shown in Table 11.

With the new group of β coefficients, using the equivalent straight cracks compared with the original straight crack, the errors can be calculated as shown in Eq. (6). The graph that correlates the error evolution for the *ASTM* method and the proposal is shown below in Fig. 15, with significant improvement when compared to the first approach. Note that even though this graph shows the error evolution for $W/B = 2$ only, $W/B = 1$ and 4 showed comparable results, which are omitted here for convenience. The strategy is then proceeded by repeating the calculations and simulations for shallow ($a/W = 0.2$, Table 12) and deep ($a/W = 0.7$, Table 13) cracks.

Three groups of linear functions that describe the β coefficients for the *SE(B) B = 25.4 mm* were generated. Since the definition of shallow, medium, and deep cracks can be arbitrary, the author decided to determine an average of the three (Table 14). The average is done by employing the least squares fit technique considering all β_i data. This procedure was done to make the proposal independent from a/W. Improvements of this methodology are being studied within the research group to make the proposal also thickness independent. For now, the main goal is to develop a group of coefficients for each thickness value for the *SE(B)*.

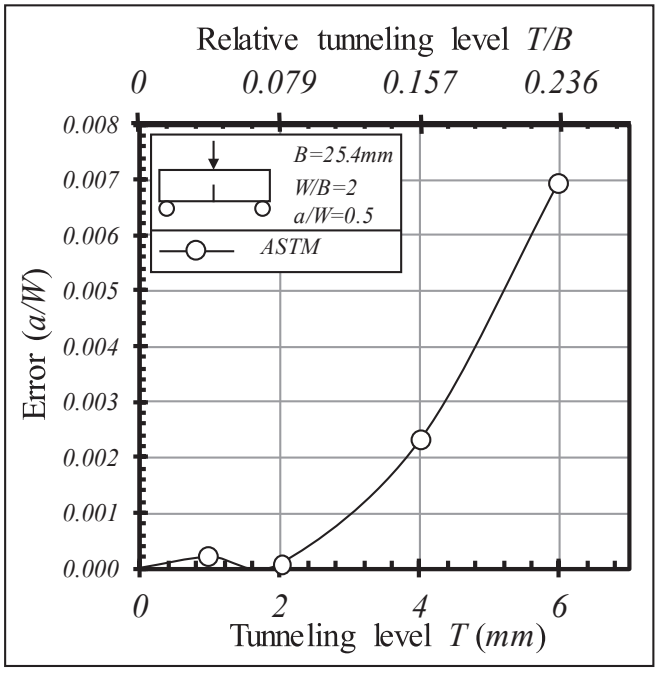

Fig. 12. Error (Eq. (6)) evolution with increasing tunneling for the ASTM method.

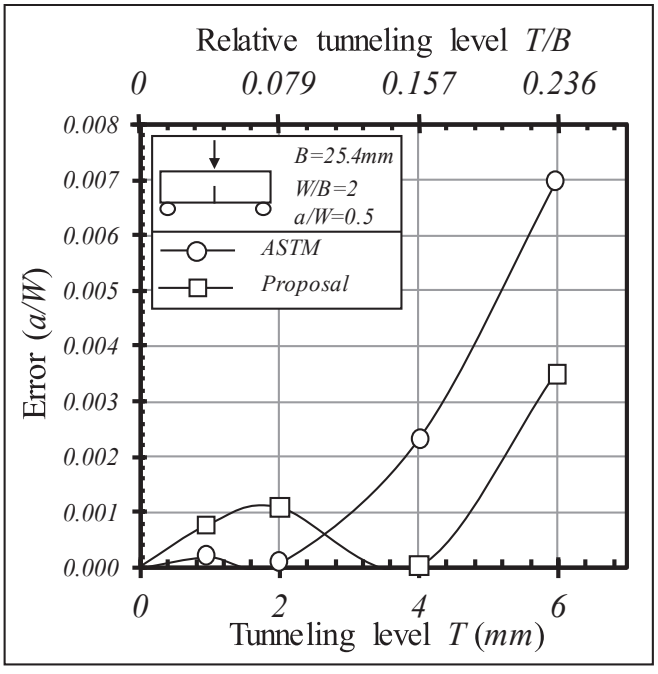

Fig. 13. Error (Eq. (6)) evolution with increasing tunneling for the ASTM method and new proposal. A substantial increase is present in the less curved cases.

Table 10
Groups of β coefficients for each tunneling level considered for the SE(B), B = 25.4 mm, a/W = 0.5.

Tunneling level T (mm)				
β_i	1	2	4	6
β_1	0.1137	0.1258	0.1547	0.1817
β_2	0.2285	0.2427	0.2737	0.3132
β_3	0.3054	0.2886	0.2465	0.2189
β_4	0.2121	0.2060	0.1947	0.1687
β_5	0.1404	0.1368	0.1303	0.1175

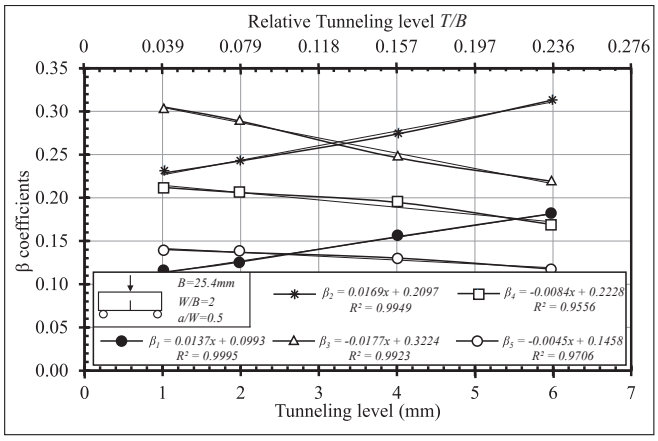

Fig. 14. Graphical representation of the β coefficients for the SE(B), B = 25.4 mm, a/W = 0.5. A linear regression with R^2 higher than 0.95 was achieved for each one.

Table 11
Group of β coefficients for all tunneling levels considered for the SE(B), B = 25.4 mm, a/W = 0.5 written as a function of the tunneling level T.

β coefficients, SE(B), B = 25.4 mm, a/W = 0.5	
β_1 = 0.0137 T + 0.0993	(edge)
β_2 = 0.0169 T + 0.2097	
β_3 = -0.0177 T + 0.3224	
β_4 = -0.0084 T + 0.2228	
β_5 = -0.0045 T + 0.1458	(center)

The same study is now repeated for the *SE(B), B = 50.8 mm* and *B = 12.7 mm*. The same strategy demonstrated above was replicated for those cases with minor modifications, as clarified below. For the *B = 50.8 mm* case, three groups of *β* coefficients were determined (*a/W = 0.2, 0.5,* and *0.7*). Following this, the average of the three was calculated and a fourth group was generated. However, the average was severely affected by the *a/W = 0.2* values as shown in Fig. 16. Since this scenario is an extreme and unlikely case, shallow crack in a thick (*W = B*) specimen with heavily tunneled crack profile, the average group was then calculated for the *a/W = 0.5* and *0.7* only (Fig. 17), and the results show that this new average is the best to describe the *SE(B) B = 50.8 mm* (Table 15).

For the *B = 12.7 mm* case, the three groups of *β* coefficients and the average of the three were determined. Again, all groups were severely affected by an extreme case. Differently from *B = 50.8 mm*, now all heavily tunneled *T = 6 mm* data deviated from a clear trend (Fig. 18). For this case, all groups of *β* coefficients were determined without the inclusion of *T = 6 mm* data (Fig. 19, Table 16).

With all the groups of *β* coefficients defined for the *SE(B), B = 50.8, 25.4,* and *12.7 mm*, the curved cracks can now be modeled and evaluated.

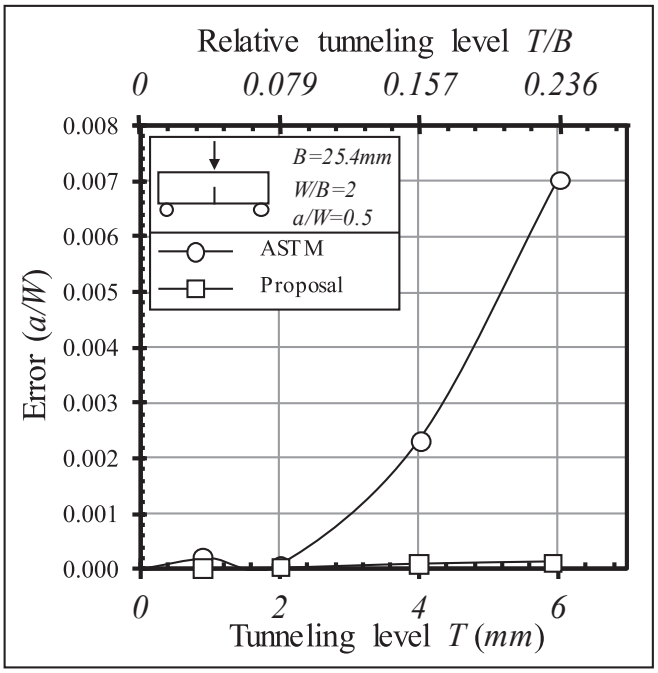

Fig. 15. Error (Eq. (6)) evolution with increasing tunneling for the ASTM method and new approach for the proposal. The error is substantially reduced.

Table 12
Group of β coefficients for all tunneling levels considered for the SE(B), B = 25.4 mm, a/W = 0.2 written as a function of the tunneling level T.

β coefficients, SE(B), B = 25.4 mm, a/W = 0.2	
β_1 = 0.0147 T + 0.1001	(edge)
β_2 = 0.0176 T + 0.2290	
β_3 = -0.0194 T + 0.3127	
β_4 = -0.0084 T + 0.2158	
β_5 = -0.0045 T + 0.1425	(center)

Table 13
Group of β coefficients for all tunneling levels considered for the SE(B), B = 25.4 mm, a/W = 0.7 written as a function of the tunneling level T.

β coefficients, SE(B), B = 25.4 mm, a/W = 0.7	
β_1 = 0.0157 T + 0.0943	(edge)
β_2 = 0.0193 T + 0.2139	
β_3 = -0.0203 T + 0.3227	
β_4 = -0.0096 T + 0.2230	
β_5 = -0.0051 T + 0.1462	(center)

Table 14
Group of β coefficients for all tunneling levels considered for the SE(B), B = 25.4 mm, a/W = 0.2, 0.5 and 0.7 (average) written as a function of the tunneling level T.

β coefficients, SE(B), B = 25.4 mm, a/W = 0.2, 0.5 and 0.7 (average)	
β_1 = 0.0147 T + 0.0979	(edge)
β_2 = 0.0179 T + 0.2175	
β_3 = -0.0191 T + 0.3192	
β_4 = -0.0088 T + 0.2205	
β_5 = -0.0047 T + 0.1448	(center)

5. Results (proposal)

Results for the proposal are displayed below. For all thicknesses evaluated for the *SE(B)*, the proposal behaved significantly better, apart from extreme cases. Independently from the error magnitudes shown in Figs. 20 to 22, results indicate that methodologies similar to the

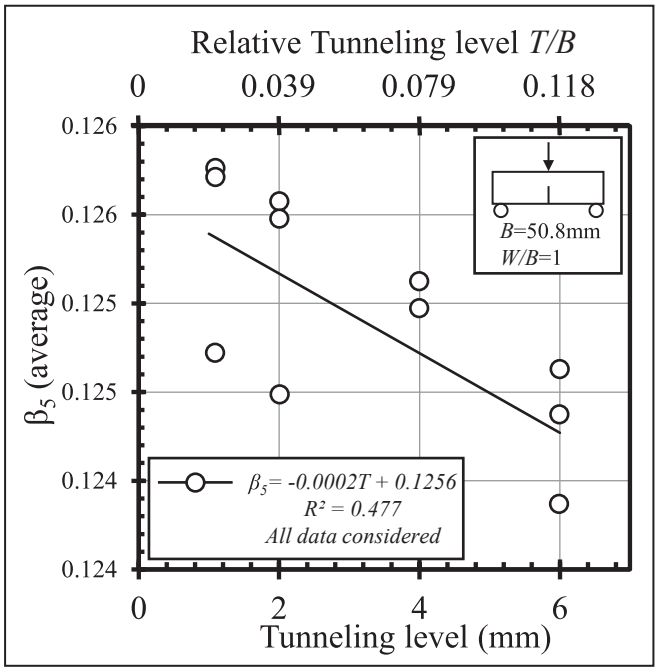

Fig. 16. β_5 (average) evolution with tunneling without excluding a/W = 0.2 data. R^2 value is 0.477.

presented in this paper are capable of developing proposals that reduce compliance errors when crack tunneling is considered and may decrease the number of invalidated results due to *ASTM* crack curvature limit violation, favoring experimental practices.

That being said, even though the proposal is specimen exclusive, thickness dependent (and therefore there are three groups of β coefficients for the *SE(B)*) and has data arbitrarily excluded from the scope of development, it presents a clear contribution for measuring the crack front and has the potential to decrease the number of specimens that violates current standards. Comparison between Tables 1 and 17 (*W/B = 1*), Tables 2 and 18 (*W/B = 2*) and tables 3 and 19 (*W/B = 4*) shows that *a/W* estimation errors with the implementation of the proposal decrease significantly (*-9.46%* on Table 3 to *−2.26%* on Table 17). Efforts within the research group are being made for developing a more robust proposal based on the strategy presented here with key modifications:

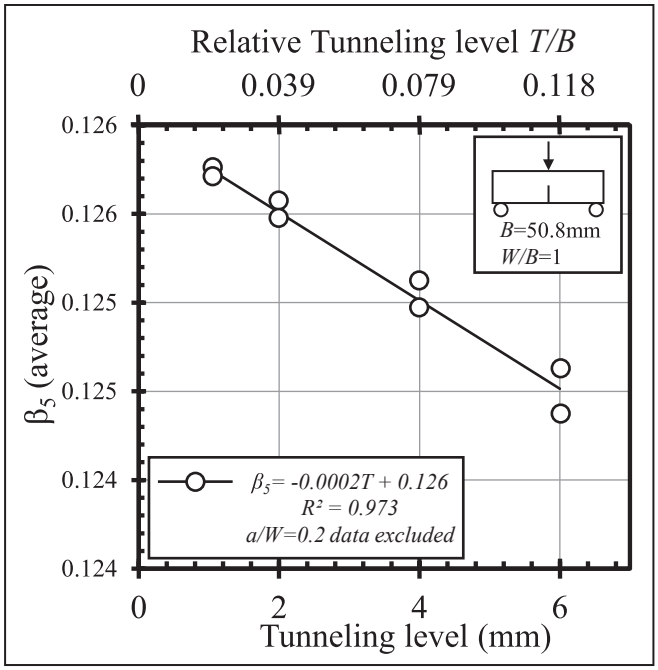

Fig. 17. β_5 (average) evolution with tunneling excluding a/W = 0.2 data. R^2 value increased from 0.477 to 0.973.

Table 15
Group of β coefficients for all tunneling levels considered for the SE(B), B = 50.8 mm, a/W = 0.5 and 0.7 (average) written as a function of the tunneling level T.

β coefficients, SE(B), B = 50.8 mm, a/W = 0.5 and 0.7 (average excluding a/W = 0.2)	
$\beta_1 = 0.0063\ T + 0.0996$	(edge)
$B_2 = 0.0095\ T + 0.2115$	
$\beta_3 = 0.0032\ T + 0.2371$	
$\beta_4 = -0.0187\ T + 0.3258$	
$\beta_5 = -0.0002\ T + 0.1260$	(center)

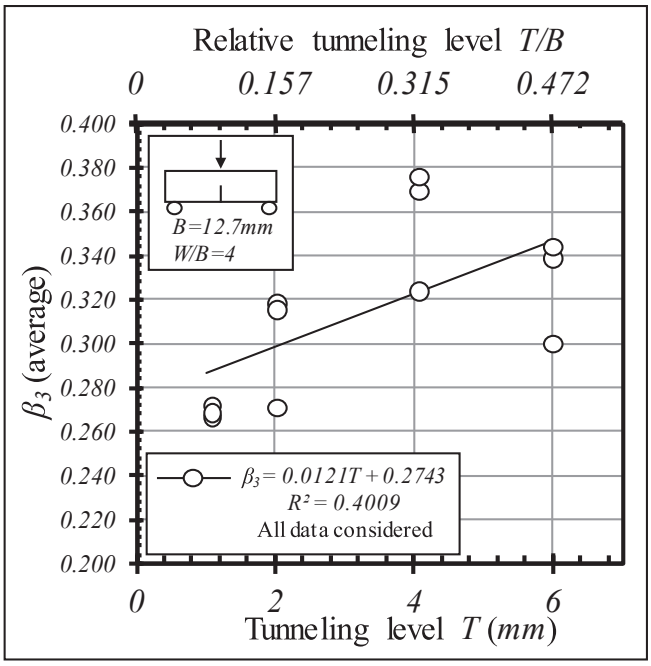

Fig. 18. β_3(average) evolution with tunneling without excluding T = 6 mm data. R^2 value is 0.4009.

- Based on relative tunneling level *T/B*;
- No arbitral exclusion of extreme data;
- Depth (*a/W*) and thickness (*B*) independent;
- Specimen independent, if possible – if not, a set of solutions for each type of specimen.

Finally, the routine for application of the proposal for a postmortem evaluation of the crack size is displayed below:

a) Determine the relative crack length a/W_i (or crack length a_i) throughout the thickness of the specimen (nine points of measurement in agreement with the *ASTM E1820* [1]);
b) Determine the tunneling level (Eq. (4));
c) Determine the points for insertion in Eq. (9). Since the proposal is based on symmetrical cracks, average the two equivalent points across the thickness of the specimen. For $1 < i < 5$: $a/W_{i\,sym}=(a/W_i + a/W_{10-i})/2)$. At this point the user should have 5 points representing 1 – edge, 2 to 4 – intermediates and 5 – center.

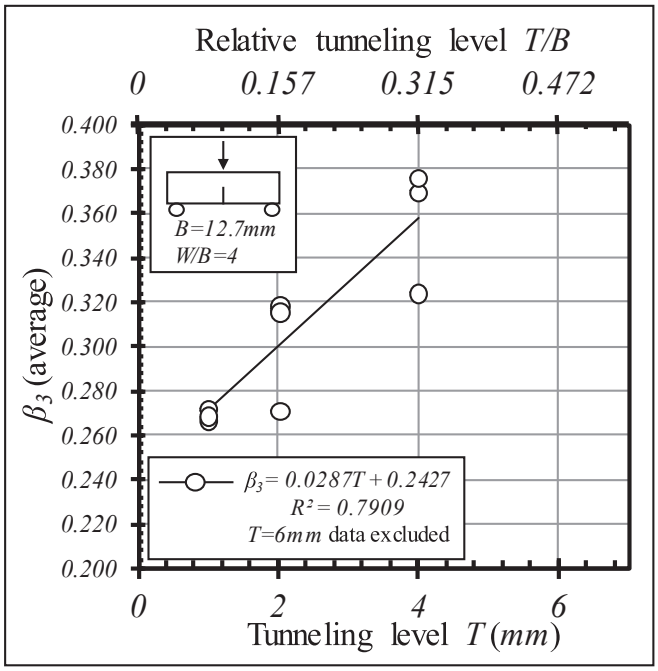

Fig. 19. β_3 (average) evolution with tunneling excluding T = 6 mm data. R^2 value increased from 0.4009 to 0.7909.

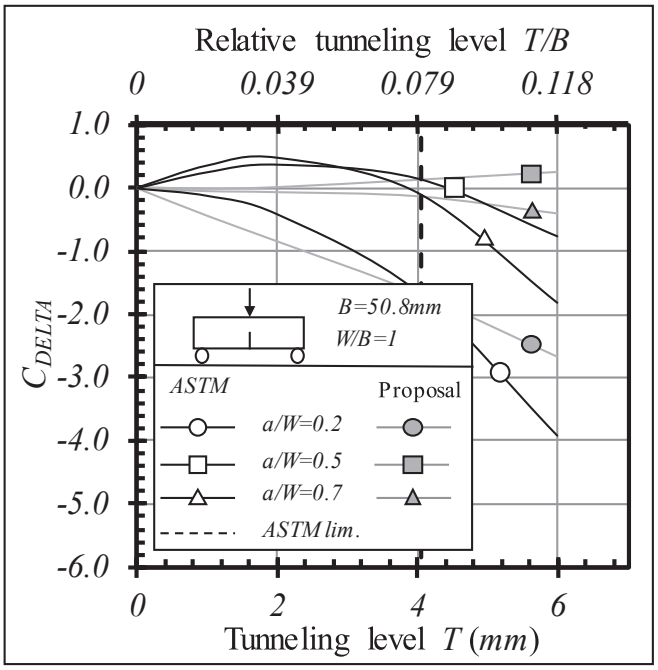

Fig. 20. Comparison between the ASTME1820 and the proposal of the compliance delta versus tunneling level for the SE(B) B = 50.8 mm.

Table 16
Group of β coefficients for all tunneling levels considered for the SE(B), B = 12.7 mm, a/W = 0.7 (excluding T = 6 mm data) written as a function of the tunneling level T.

β coefficients, SE(B), B = 25.4 mm, a/W = 0.2, 0.5 and 0.7 (average, excluding T = 6 mm data)	
β_1 = 0.0275 T + 0.1085	(edge)
β_2 = 0.0343 T + 0.2415	
β_3 = -0.0262 T + 0.2826	
β_4 = -0.0250 T + 0.2325	
β_5 = -0.0106 T + 0.1349	(center)

d) Apply the following Eq. (7) with adequate β coefficients for each thickness ($B = 25.4\ mm$ Table 14, $B = 50.8\ mm$ Table 15, $B = 12.7\ mm$ Table 16).
e) Apply the resulting equivalent a/W for fracture mechanics calculations.

$$a/W_{eq.sym.} = \sum_{i=1}^{5} \beta_i a/W_{i\_sym} \tag{9}$$

6. Conclusions

Part 1: Compliance changes due to tunneling.

- Reduced deviations on compliance (under ± 0.5%) were detected within ASTM crack curvature limits for all studied cases. However, as tunneling increases and violates these limits, remarkable compliance errors take place, which is consistent with the literature [18–19]. In extreme cases of this paper, those represent C_{DELTA} up to -13.67% (Table 3) and a/W_{DELTA} up to -10.63% (Table 9), potentially affecting fracture mechanics test results that are dependent of the instantaneous crack size such as *J-R* and *da/dN vs. ΔK*.
- The same behavior of compliance evolution with increasing tunneling was observed for *C(T), SE(B),* and $SE(T)_c$ geometries. This may indicate that this phenomenon affects all studied specimens in the same way, regardless of loading profile and *W/B* relationship. Further investigation on this topic may be relevant.
- When modeled with the *ASTM E1820* method [1], with increasing curvature, the center portion of the crack tends to get deeper and the edges, shallower. This combination favors the decrease in compliance for tunneling levels above the *ASTM* limit as shown in Figs. 2 to 10.

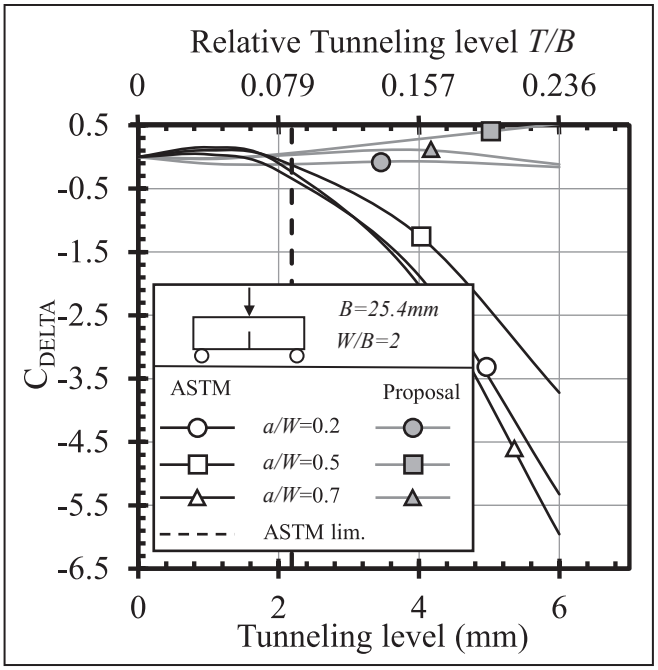

Fig. 21. Comparison between the ASTM E1820 and the proposal of the compliance delta versus tunneling level for the SE(B) B = 25.4 mm.

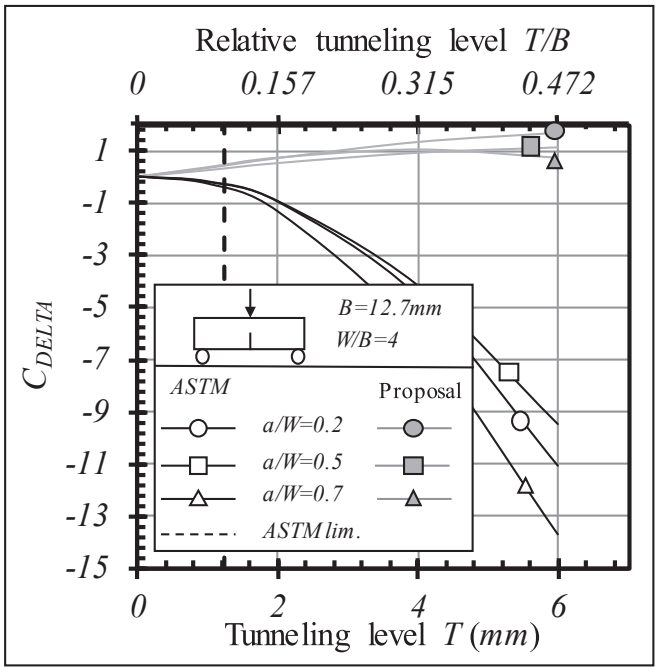

Fig. 22. Comparison between the ASTM E1820 and the proposal of the compliance delta versus tunneling level for the SE(B) B = 12.7 mm.

Table 17
Proposal results for SE(B) specimen, W/B = 1. All a/W and T levels.

Model a/W	T level	Compliance	C_{DELTA}	$a/W_{predicted}$	a/W_{DELTA}
(mm/mm)	(mm)	(mm/N)	%	(mm/mm)	%
0.2	0	6.42E-07	n/a	0.192	n/a
	1	6.39E-07	−0.44	0.191	−0.37
	2	6.37E-07	−0.84	0.190	−0.71
	4	6.32E-07	−1.67	0.189	−1.41
	6	6.25E-07	−2.68	0.187	−2.26
0.5	0	3.20E-06	n/a	0.488	n/a
	1	3.20E-06	−0.02	0.488	−0.01
	2	3.20E-06	0.00	0.488	0.00
	4	3.20E-06	0.12	0.489	0.05
	6	3.21E-06	0.25	0.489	0.09
0.7	0	1.14E-05	n/a	0.690	n/a
	1	1.14E-05	−0.04	0.690	−0.01
	2	1.14E-05	−0.06	0.690	−0.01
	4	1.14E-05	−0.12	0.690	−0.02
	6	1.14E-05	−0.40	0.690	−0.08

Table 18
Proposal results for SE(B) specimen, W/B = 2. All a/W and T levels.

Model a/W	T level	Compliance	C_{DELTA}	$a/W_{predicted}$	a/W_{DELTA}
(mm/mm)	(mm)	(mm/N)	%	(mm/mm)	%
0.2	0	1.32E-06	n/a	0.196	n/a
	1	1.32E-06	−0.11	0.196	−0.09
	2	1.32E-06	−0.12	0.196	−0.10
	4	1.32E-06	−0.07	0.196	−0.06
	6	1.32E-06	−0.16	0.196	−0.13
0.5	0	6.56E-06	n/a	0.493	n/a
	1	6.56E-06	−0.02	0.493	−0.01
	2	6.56E-06	0.04	0.493	0.01
	4	6.58E-06	0.28	0.493	0.10
	6	6.59E-06	0.53	0.494	0.19
0.7	0	2.35E-05	n/a	0.693	n/a
	1	2.35E-05	−0.03	0.693	−0.01
	2	2.35E-05	0.02	0.693	0.00
	4	2.35E-05	0.11	0.693	0.02
	6	2.34E-05	−0.12	0.693	−0.02

Table 19
Proposal results for SE(B) specimen, W/B = 4. All a/W and T levels.

Model a/W	T level	Compliance	C_{DELTA}	$a/W_{predicted}$	a/W_{DELTA}
(mm/mm)	(mm)	(mm/N)	%	(mm/mm)	%
0.2	0	2.68E-06	n/a	0.198	n/a
	1	2.69E-06	0.34	0.199	0.28
	2	2.70E-06	0.73	0.200	0.60
	4	2.71E-06	1.36	0.201	1.12
	6	2.72E-06	1.72	0.201	1.41
0.5	0	1.33E-05	n/a	0.495	n/a
	1	1.33E-05	0.25	0.495	0.09
	2	1.33E-05	0.54	0.496	0.19
	4	1.34E-05	0.95	0.497	0.34
	6	1.34E-05	1.16	0.497	0.42
0.7	0	4.77E-05	n/a	0.696	n/a
	1	4.79E-05	0.38	0.696	0.07
	2	4.81E-05	0.76	0.697	0.14
	4	4.82E-05	1.09	0.697	0.20
	6	4.81E-05	0.75	0.696	0.14

Part 2: A new approach for measuring the equivalent crack size.

- The exploratory proposal for measuring and post-processing the curved crack profile of fracture mechanics specimens is presented. Even though there are limitations, results show that the strategy can lead to reduced deviations and increased scope of validity for tunneled fracture specimens.
- This paper indicates that current results are useful for SE(B) testing with enhanced efficiency and accuracy, but there is an opportunity for developing a more comprehensive proposal – independent of crack size, thickness and, if possible, specimen type – that incorporates the effects of crack tunneling on compliance. These efforts are being made within the research group.
- This paper does not address the tunneling effects on crack driving forces directly and focuses only on the crack estimation by the compliance technique. It is worth noting that additional efforts regarding the effects of the developed proposals on crack driving forces are of paramount relevance and will also be addressed in further investigations.

CRediT authorship contribution statement

L.G.F. Andrade: Conceptualization, Methodology, Software, Investigation, Writing – original draft. **M. Mattar Neto:** Formal analysis, Writing – review & editing. **G.H.B. Donato:** Writing – review & editing, Supervision.

Declaration of Competing Interest

The authors declare that they have no known competing financial interests or personal relationships that could have appeared to influence the work reported in this paper.

Data availability

Data will be made available on request.

Acknowledgements

The authors would like to acknowledge *CNPQ* (grant *486176/2013-4*), *CAPES* and *FEI* University for all the support given to complete this work.

References

[1] American Society for testing and materials. ASTM E 1820: Standard test method for measurement of fracture toughness, Philadelphia, 2022.

[2] American Society for testing and materials. ASTM E 647: Standard test method for measurement of fatigue crack growth rates, Philadelphia, 2015.
[3] American Society for testing and materials. ASTM E 399: Standard test method for linear-elastic plane-strain fracture toughness of metallic materials, Philadelphia, 2022.
[4] T.L. Anderson, Fracture mechanics, 3. ed., Taylor & Francis Group, New York, 2005.
[5] G.A. Clarke, et al. Single specimen tests for JIC determination. mechanics of crack growth, ASTM STP 590. p. 27–42, Philadelphia, 1976.
[6] R.L. Tobler, W.C. Carpenter, A numerical and experimental verification of compliance functions for compact specimens, Eng. Fract. Mech. 21 (3) (1985) 547–556.
[7] B.K. Neale, R.H. Priest, The unloading compliance method for crack length measurement using compact tension and preckracked charpy specimens, in: E. T. Wessel, F.J. Loss (Eds.), ASTM STP 856 - Elastic-plastic fracture test methods: The user's experience, Library of Congress, Philadelphia, 1985, pp. 375–393.
[8] D.A. Jablonski, et al., Compliance functions for various fracture mechanics specimens, Eng. Fract. Mech. 22 (1985) 819–827.
[9] S.X. Wu, Crack length calculation formula for three point bend specimens, Int. J. Fract. 24 (1984) R33–R35.
[10] S. Cravero, R. Bravo, H. Ernst, Constraint evaluation and effects on J-R resistance curves for pipes under combined load conditions, in: 17TH European conference on fracture, 2008, Brno.
[11] F.C. Moreira, G.H.B. DONATO, Effects of side-grooves and 3-D geometries on compliance solutions and crack size estimations applicable to C(T), SE(B) and clamped SE(T) specimens, in: Proceedings of the ASME 2013 pressure vessels & piping division. Paris, France, 2013.
[12] British Institution, Method of test for determination of fracture toughness in metallic materials using single edge notched tension (SENT) specimens. BS 8571, 2018.
[13] Det Norske Veritas, DNV-RP-F108: Fracture control for pipeline installation methods introducing cyclic plastic strain, Høvik, 2006.
[14] CANMET, Recommended practice: fracture toughness testing using SE(T) samples with fixed-grip loading, CANMET Materials Technology Laboratory, Ottawa, 2010.
[15] Exxon Mobil, Measurement of crack tip opening displacement (CTOD) – fracture resistance curves using single-edge notched tension (SENT) specimens, ExxonMobil Upstream Research Company, Houston, 2010.
[16] G. Shen, W.R. Tyson, Crack size evaluation using unloading compliance in single specimen Single-Edge-Notched tension fracture toughness testing, J. Test. Eval. 37 (4) (2009).
[17] M.A. Verstraete, et al., Evaluation and interpretation of ductile crack extension in sent specimens using unloading compliance technique, Eng. Fract. Mech. 115 (2014) 190–203.
[18] Z. Yan, W. Zhou, Effect of crack front curvature on CMOD compliance and crack length evaluation for single-edge bend specimens, in: Proceedings of the Canadian society for mechanical engineering international congress, 2014.
[19] Y. Huang, W. Zhou, Effects of crack front curvature on J-R curve testing using clamped SE(T) specimens of homogeneous materials, Int. J. Press. Vessel. Pip. 134 (2015) 112–127.
[20] P. Steenkamp, JR-curve testing of three-point bend specimens by the unloading compliance method, in: Fracture mechanics: Eighteenth symposium, ASTM STP 945, p. 583-610. Philadelphia, 1988.
[21] G. Nikishkov, J. Heerens, D. Hellmann, Effect of crack front curvature and side grooving on CTOD δ5 and J-integral in CT and 3PB specimens, J. Test. Eval. JTEVA 27 (5) (1999) 312–319.
[22] E. Wang, et al., Numerical study on CMOD compliance for single-edge notched bending specimens, J. Press. Vessel. Technol. v (2016) 138.
[23] K. Van Minnebruggen, et al., Crack growth characterization in single-edge notched tension testing by means of direct current potential drop measurement, Int. J. Press. Vess. Pip. (2017).
[24] J. Tang, et al., Evaluation of fracture toughness in different regions of weld joints using unloading compliance and normalization method, Eng. Fract. Mech. v (2018) 195.
[25] B.D. Snartland, C. Thaulow, Fracture toughness testing at the micro-scale – The effect of the unloading compliance method, Eng. Fract. Mech. v (2020) 235.
[26] R.F. de Souza, C. Ruggieri, Revised wide range compliance solutions for selected standard and non-standard fracture test specimens based on crack mouth opening displacement, Eng. Fract. Mech. (2017).
[27] L.G.F. Andrade, G.H.B. Donato, Effects of crack tunneling and plasticity on the elastic unloading compliance technique for SE(B) – current limitations and proposals, Proc. Struct. Integr. (2018).
[28] Simulia, Abaqus theory guide. [S.I.]. Abaqus Software Documentation, v.6.20, 2020.